Validation of Non-darcy Well Models Using Direct Numerical Simulation

Chapter *in* Lecture Notes in Physics · January 2008

DOI: 10.1007/3-540-45467-5_12

5 authors, including:

Vladimir A. Garanzha
Russian Academy of Scie…
34 PUBLICATIONS **108** CITATIONS
SEE PROFILE

Guan Qin
University of Houston
56 PUBLICATIONS **655** CITATIONS
SEE PROFILE

Validation of Non-darcy Well Models Using Direct Numerical Simulation

Vladimir A. Garanzha Vladimir N. Konshin
Stephen L. Lyons Dimitrios V. Papavassiliou
Guan Qin

Abstract

We describe discrete well models for 2-D non-Darcy fluid flow in anisotropic porous media. Attention is mostly paid to the well models and simplified calibration procedures for the control volume mixed finite element methods, including the case of highly distorted grids.

KEYWORDS: well models, non-Darcy flows, anisotropy, distorted grids

1 Introduction

Flow around high production rate gas wells deviates from Darcy's law. This phenomenon has been successfully modeled by the two-term Forchheimer law [7].

In reservoir simulation, the discrete well model is a relation between the production/injection rate of the well, the well-block pressure and the bottom-hole pressure. This relation is specific to the basic approximation scheme used for discretizing the governing equations. Such well models are well understood in the case of Darcy flow and are mostly based on various generalizations of the effective radius concept [1, 10]. In the case of Forchheimer flow in isotropic media, we find the effective radius as a function of the dimensionless Forchheimer number using the invariant behavior of discrete solutions near the well blocks. Such invariant properties are analyzed in [6] and are assessed numerically by solving a set of auxiliary problems which reproduce the known analytical solutions around a single isolated well in an infinite domain. Our numerical experiments show that this calibration procedure is very accurate and can also be applied on non-uniform and highly distorted grids.

In the general case of anisotropic media, there is no consensus on a specific formulation of Forchheimer's law that is backed by experiments or from

Z. Chen, R.E. Ewing, and Z.-C. Shi (Eds.): Proceedings 1999, LNP 552, pp. 156–169, 2000.

first principles. In this work, we derive well models only for the simplest formulation [9], which provides reasonably good fit to pore network simulation results such as those obtained by Thauvin and Mohanty [14].

In this case direct numerical simulation becomes a critical tool for estimating the validity of a specific well model. Such verification requires much higher accuracy compared to conventional reservoir simulation techniques and imposes strict requirements on the quality of the approximation scheme. To this end we have developed a modification of the control volume mixed finite element (CVMFE) scheme [4] based on quadrilateral grids in 2-D and on hexahedral grids in 3-D. This scheme is conservative, nearly optimal among second order schemes, and naturally incorporates harmonic averaging of reservoir properties. Moreover it allows us to obtain reliable results on highly distorted grids and even on grids that are "degenerate" in the conventional finite element sense (for example on grids with non-convex cells in the plane.)

Numerical experiments in the 2-D case show that very fine grids are necessary in order to obtain grid independent results using direct simulation. Such grids may be impractical in the 3-D case, especially in the case of deviated wells. Hence there is a need for high order methods suitable for accurate resolution of the flow in the near-well region using coarse grids.

2 Problem Formulation and Governing Equations

The governing equations that describe steady-state, single-component, single phase, isothermal flow in porous media are

$$\nabla \cdot (\rho \mathbf{u}) = f, \quad \mu K^{-1}\mathbf{u} + \rho\beta|\mathbf{u}|\mathbf{u} + \nabla p = 0, \tag{2.1}$$

where ρ denotes the fluid density, $\mathbf{u}$ the velocity vector, μ the dynamic viscosity and p the pressure. The porous medium is characterized by the permeability tensor K, the porosity ϕ and the Forchheimer coefficient β, which can be a tensor in some formulations. The right hand side f is associated with the presence of wells-localized mass inflows or outflows in the reservoir.

Different Forchheimer law formulations are available for the anisotropic case. Thauvin and Mohanty, [14], require that $\beta = \{b_{ij}\}$ in order to fit their network simulation results. Knupp and Lage [9] have suggested an anisotropic formulation using a variational approach. Their formulation can be written

as follows

$$\mu K^{-1}\mathbf{u} + \beta\rho\frac{(\mathbf{u}\cdot K^{-1}\mathbf{u})^{\frac{1}{2}}}{(\det K^{-1})^{\frac{3}{2n}}}K^{-1}\mathbf{u} + \nabla p = 0, \quad n = 2,3, \ \beta \ \text{ is scalar}, \qquad (2.2)$$

where $n = 2,3$ is the space dimension. This model has fewer degrees of freedom as compared to (2.1). Nevertheless, it provides a good fit to the data from [14]. However, these data are still not enough in order to choose a particular tensorial model.

3 CVMFE on Distorted Quadrilateral Grids

In order to describe the discrete approximation to system (2.1) on quadrilateral grids for each element we introduce the mapping $\mathbf{r} = \mathbf{r}(\xi_1, \xi_2)$ which maps the unit square on the quadrilateral in physical coordinates $\mathbf{r} = (x_1, x_2)^T$ and associated metric entities

$$\mathbf{g}_i = \frac{\partial \mathbf{r}}{\partial \xi_i}, \quad S = \{s_{ij}\}, \quad s_{ij} = \frac{\partial x_i}{\partial \xi_j}, \quad J = \det S, \quad \mathbf{g}_j^T\mathbf{g}^i = J\delta_{ij},$$

where $\mathbf{g}_i, \mathbf{g}^i$ are the covariant and scaled contravariant basis vectors and J is the Jacobian of the mapping. Using above notations the governing equations can be written as follows:

$$\sum_{i=1}^{n}\frac{\partial}{\partial \xi_i}\rho V^i = Jf, \qquad (3.1)$$

$$\sum_{j=1}^{n}\frac{1}{J}\mathbf{g}_i^T\left(\mu I + \beta\rho\frac{(\mathbf{u}\cdot K^{-1}\mathbf{u})^{\frac{1}{2}}}{(\det K^{-1})^{\frac{3}{2n}}}\right)K^{-1}\mathbf{g}_j V^j + \frac{\partial}{\partial \xi_i}p = 0 \qquad (3.2)$$

$$V^i = \mathbf{u}^T\mathbf{g}^i, \quad \mathbf{u} = \frac{1}{J}\sum_{i=1}^{n}\mathbf{g}_i V^i \ \text{ (Piola mapping)}.$$

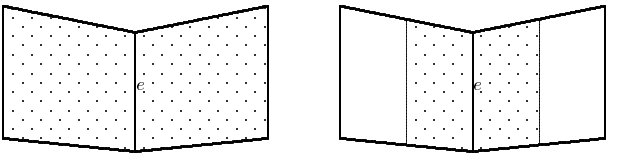

Figure 1: Support for the edge-centered flux base $\boldsymbol{\phi}_e$ (left) and for the flux test function $\boldsymbol{\psi}_e$ (right).

The Control Volume Mixed Finite Element methods (CVMFE) as introduced in [4] are based on the lowest order Raviart-Thomas (RT_0) flux basis functions and cell-based pressures. Equation (3.1) is integrated over the grid cell in the parametric space with mid-point quadrature rules for the contour integrals. The Forchheimer law (3.2) is integrated over the edge-centered control volumes in the parametric space and mid-point rules are used for pressure contour integrals. This derivation is equivalent to using the Raviart-Thomas flux-pressure bases, piecewise-constant pressure test functions and flux test functions $\boldsymbol{\psi}_e$ defined by (3.3), which is illustrated on Fig. 1 for the cases when the edge e locally coincides with the vector $\mathbf{g}_2$.

$$\boldsymbol{\phi}_e = \begin{cases} (1-\xi_1)\frac{1}{J}\mathbf{g}_1 & \text{in} \quad c_{\text{right}}(e) \\ \xi_1 \frac{1}{J}\mathbf{g}_1 & \text{in} \quad c_{\text{left}}(e) \\ 0 & \text{elsewhere} \end{cases} \qquad \boldsymbol{\psi}_e = \begin{cases} \frac{1}{J}\mathbf{g}_1 & \text{in} \quad c_{\text{right}}(e) \\ \frac{1}{J}\mathbf{g}_1 & \text{in} \quad c_{\text{left}}(e) \\ 0 & \text{elsewhere} \end{cases} \tag{3.3}$$

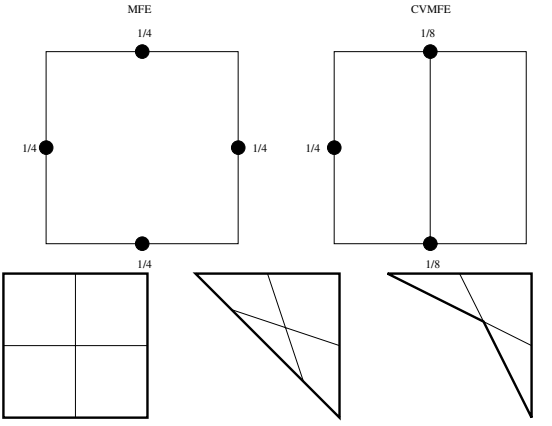

Figure 2: Equivalent first order quadrature rules and distorted grid cells.

In [4] the value $\frac{1}{J}$ is in fact approximated by a constant in each half-cell which allows the integrals over cells to be computed exactly. The basic advantage of CVMFE is the observed $O(h^2)$ convergence [4] in terms of pressure and fluxes on highly nonuniform grids and in the presence of strong coefficient jumps. Moreover it possesses optimal spectral resolution properties in a whole range of the discrete harmonics and provides accurate solutions on mildly distorted grids. The main drawbacks of CVMFE are the lack of the Linear Preservation (LP) property and nonsymmetric discrete metric tensor.

It is possible to derive CVMFE alternatively as a "low order" approximation to conventional mixed finite element (MFE) method [12]. Thorough

analysis of relations between finite volume and finite element methods with different quadrature rules can be found in [2] where it was shown that most FE methods in primal and dual formulations can be written in the "factorized" form, or as a flux differences in terms of finite volume methods.

In [8] it was shown that there exist quadrature rules for the MFE integrals with first order algebraic accuracy which result in partial error cancellation property, namely they result in the discrete system which is identical to that resulting from RT_0 bases and flux test functions defined by (3.3) with certain first order quadrature rules, which are shown on Fig. 2.

The resulting discrete system coincides with CVMFE [4] on grids with affine cells, the discrete metric tensor is symmetric positive definite on admissible cells. Moreover the scheme is Linearity Preserving and is more accurate than the original CVMFE on distorted grids. The set of admissible grids is wider for this scheme as compared to conventional finite elements in the following sense: the necessary condition for the convergence of discrete solutions in the case $\beta = 0$ in fully discrete norms is that the Jacobian of the local mapping in the cell edge centers is bounded from below by a positive constant (see Fig. 2). The convergence proof is similar to that in [13] and the invertibility of local mapping for each element is not required, i.e., the cell shown on Fig. 2 (center), is admissible and the local discrete metric tensor is positive definite and has condition number of the order of unity in this case. An example of degenerate cell is shown on Fig. 2 (right).

Similar conclusions are valid in the primal formulation, i.e., for the bilinear finite element method and control volume finite element method.

4 Analytical Estimates for the Equivalent Well-Block Radius r_0 in Isotropic Darcy Flow

In the case of infinite uniform grid with square cells and isotropic Darcy flow the generic dimensionless discrete system which comprises several well known approximation schemes can be written as follows:

$$\begin{aligned}
&-(2+2w)P_{ij} + w(P_{i-1\,j} + P_{i+1\,j} + P_{i\,j-1} + P_{i\,j+1}) \\
&+\tfrac{1-w}{2}(P_{i-1\,j-1} + P_{i+1\,j-1} + P_{i-1\,j+1} + P_{i+1\,j+1}) = \\
&sQ_{ij} + (1-s)\left(\tfrac{36}{64}Q_{ij} + \tfrac{6}{64}(Q_{i-1\,j} + Q_{i+1\,j} + Q_{i\,j-1} + Q_{i\,j+1})\right. \\
&\left. + \tfrac{1}{64}(Q_{i-1\,j-1} + Q_{i+1\,j-1} + Q_{i-1\,j+1} + Q_{i+1\,j+1})\right),
\end{aligned} \tag{4.1}$$

where i, j are the grid node(cell) indices.

We seek the solution P_{ij} to (4.1) in the infinite computational domain $-\infty \le i, j \le +\infty$ with the following right hand side Q

$$Q_{00} = 1, \quad Q_{ij} = 0, \; i^2 + j^2 > 0. \tag{4.2}$$

The problem (4.1),(4.2) is closed with the following condition

$$P_{00} = 0, \quad \lim_{r\to\infty} \frac{P_{ij}}{r} = 0, \quad r = \Delta x\sqrt{i^2 + j^2}, \tag{4.3}$$

where Δx is the side of the square grid cell.

The solution to problem (4.1)–(4.3) exists and is unique [1]. Similar to [1] our objective is to find the value r_0 such that the following equality is valid

$$\lim_{r\to\infty} (P_{ij} - \frac{1}{2\pi} \ln \frac{r_0}{r}) = 0, \quad r = \Delta x\sqrt{i^2 + j^2}. \tag{4.4}$$

Equation (4.1) leads to some popular schemes, in particular the values $s = 1, w = 1$ correspond to conventional finite difference scheme (FD), $s = 0, w = \frac{1}{3}$ is the bilinear finite element (BFE) scheme, while $s = 0, w = \frac{1}{2}$ correspond to the control volume finite element method (CVFE) and the control volume mixed finite element method (CVMFE). In the latter case equation (4.1) is deduced from the extended system by elimination of flux variables. In order to underline the difference between the single-cell production term and multiple-cell production term we include the schemes CVFE' and BFE' which are defined by the parameters $s = 1, w = \frac{1}{2}$ and $s = 1, w = \frac{1}{3}$, respectively.

Andreev [1] derived the asymptotic expansion for the case $s = 1$. It can be generalized for the general case $s \ne 1$ by adding a constant c,

$$P_{ij} = c + \frac{1}{2\pi}(\ln \frac{\Delta x}{r} - \frac{3}{2} \ln 2 - \gamma + \frac{1}{2} \ln w) + O\left(\frac{\Delta x^2}{r^2}\right), r = \Delta x\sqrt{i^2 + j^2},$$

where $\gamma = 0.57722156649\ldots$ is the Euler constant. The value of c for several approximation schemes was computed in [8] using the analytical solutions from [1] and superposition principle. Comparing the above equality with (4.4) we obtain that

$$\frac{r_0}{\Delta x} = e^{-\gamma - \frac{3}{2}\ln 2 + \frac{1}{2}\ln w + 2\pi c},$$

A simple approximate solution approach for finding r_0 was suggested in [10] using the observation that discrete solution in the near well cells is close to the analytical solution. Omitting the derivation details we obtain

$$\frac{r_0}{\Delta x} = e^{-\frac{\pi}{1+w}(s+(1-s)\frac{9}{16})+\frac{1-w}{2(1+w)}\ln 2}.$$

All results are summarized in Table 1.

Scheme	$\frac{r_0}{\Delta x}$, exact value	exact value	$\frac{r_0}{\Delta x}$, Peaceman	error %
BFE	$\frac{(2+\sqrt{3})\,\frac{5\sqrt{3}}{16}\,e^{-\gamma+\frac{3\pi}{32}}}{2\sqrt{6}}$	0.313833	$2^{1/4}\,e^{-27\pi/64}$	0.68
BFE'	$\frac{e^{-\gamma}}{2\sqrt{6}}$	0.114607	$2^{1/4}\,e^{-3\pi/4}$	1.65
FD	$\frac{e^{-\gamma}}{2\sqrt{2}}$	0.198506	$e^{-\pi/2}$	4.72
CVMFE	$\frac{1}{4}\,e^{\frac{1}{8}(4-8\gamma+\pi)}$	0.3427305	$2^{1/6}\,e^{-3\pi/8}$	0.83
CVFE'	$\frac{e^{-\gamma}}{4}$	0.140365	$2^{1/6}\,e^{-2\pi/3}$	1.52

Table 1. Equivalent radius for different numerical schemes and Darcy flow.

5 Calibration Procedure Based on the Solution of Auxiliary Problem

The equivalent radius does depend on the discrete representation of point sources/sinks. The most natural discrete approximation to the δ-function is by the piecewise-constant hat function, which is illustrated in Fig. 3. Rigorous analysis and convergence proofs for such approximations as applied to the Darcy law case can be found in [5]. We write the contribution to the right hand side f in (2.1) from a single well as follows

$$f = \frac{Q}{H}\phi(\mathbf{r}-\mathbf{r}_0),$$

$$\phi(\mathbf{r}) = \begin{cases} \frac{(\lambda_1+\lambda_2)^2}{4d^2\lambda_1\lambda_2}, & \mathbf{r}\in\Omega_h(K) \\ 0, & \mathbf{r}\notin\Omega_h(K) \end{cases}, \quad \Omega_h(K) = \{\mathbf{r} : |\mathbf{a}_i\cdot\mathbf{r}| < \frac{d\lambda_i}{\lambda_1+\lambda_2}\}.$$

Here $\mathbf{r}_0$ is the well location, H is the height of the perforated zone (fully penetrating vertical wells are assumed), Q is the mass rate of the well, $\mathbf{a}_i, \lambda_i$ are the unit eigenvector and eigenvalue of K in the vicinity of the well, respectively, or

$$K = A\Lambda A^T,\ A = (\mathbf{a}_1, \mathbf{a}_2),\ \Lambda = \mathrm{diag}(\lambda_i),\ A^TA = I,$$

while d is chosen such that the well block can be placed inside $\Omega_h(K)$, e.g., on square grid $d = \Delta x$.

The reason for this choice of hat function is that it is non-zero in the square in the transformed coordinates

$$\mathbf{r}' = \Lambda^{-\frac{1}{2}}A^T\mathbf{r}. \tag{5.1}$$

This typically results in multiple-cell production terms for a single well and the estimates for r_0 differ from those in [1] and [11] since the superposition principle should be used for its computation in the linear case.

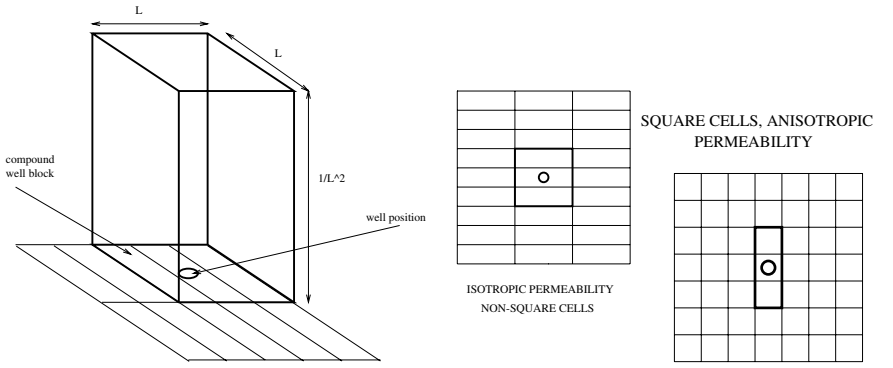

Figure 3: Discrete approximation to the production terms.

The basic motivation for this model of discrete sources and sinks is that numerical solutions in the vicinity of the well are more accurate compared to single-cell production term (typically by factor 4 to 7 on the grid with 1:3 aspect ratio shown on Fig. 3.

The well models in the case of isotropic Forchheimer flow are based on the analytical solution for radial flow around isolated well [3]

$$p(r) = p_R + \frac{\mu}{k\rho}\frac{Q}{2\pi H}\ln\left(\frac{r}{R}\right) + \frac{\beta Q|Q|}{\rho(2\pi H)^2}\left(\frac{1}{R} - \frac{1}{r}\right), \tag{5.2}$$

Using the assumption that the finite difference solution in the cells near the well block is close to the analytical solution (5.2), it was shown in [6] that the local behavior of the discrete solution is described by the dimensionless Forchheimer number of the well block defined as $Fo = \frac{\beta k|Q|}{4\Delta x \mu H}$. The equivalent radius $\alpha = r_0/\delta x$ was found as a solution to the nonlinear equation

$$\frac{\pi}{2}(1 + Fo) = \ln\left(\frac{1}{\alpha}\right) + \frac{2}{\pi}Fo\left(\frac{1}{\alpha} - 1\right),$$

In [6] the well model was derived also for the bilinear finite element approximations, or BFE′ in our notations since single-cell production term was used. The result looks as follows

$$p_0 = p_w + \frac{\mu}{k\rho}\frac{Q}{2\pi H}\ln\left(\frac{r_w}{\alpha_1\Delta x}\right) + \frac{\beta Q|Q|}{\rho(2\pi H)^2}\left(\frac{1}{\alpha_2\Delta x} - \frac{1}{r_w}\right),$$

where p_0, p_w are the well block pressure and flowing well pressure, respectively, $\alpha_1 = 2^{\frac{1}{4}}e^{\frac{-3\pi}{4}}$ (see the same value in Table 1), $\alpha_2 = \frac{8(\Gamma+\sqrt{2})}{4(\Gamma+\sqrt{2})(1+\frac{1}{\sqrt{2}})+9\pi^2}$, and $\Gamma \approx 1.35$ is the empirical calibration constant. The above results have

provided insight into the problem, however they cannot be used in the case of irregular and distorted grids. To this end we suggest to find r_0 via solution of small auxiliary system using the following procedure:

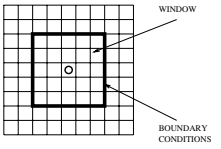

Figure 4.

(a) choose a window around the well block; (b) write discrete approximation to governing equations in this window; (c) specify Dirichlet boundary conditions using the analytical solution (5.2); (d) solve discrete system, find the pressure in the well block p_0 and find r_0 via $\frac{r_0}{R} = e^{(p_0 - p_R)\frac{2\pi H k \rho}{\mu Q}}$

Choosing the window size to be 3×3 cells results in accuracy which is comparable to that of the Peaceman method while using well block plus 2 cells in each direction typically allows to obtain 3 to 4 correct digits in r_0.

An attractive feature of this simple calibration procedure is that it can be used in the case of anisotropic permeability using the following analytical solution to (2.1) and (2.2)

$$p(\tilde{r}) = p_R + \frac{\mu}{(\det K)^{\frac{1}{2}}\rho}\frac{Q}{2\pi H}\ln\left(\frac{\tilde{r}}{R}\right) + \frac{\beta Q|Q|}{\rho(2\pi H)^2}\left(\frac{1}{R} - \frac{1}{\tilde{r}}\right),\ \tilde{r} = \frac{(\mathbf{r}^T K^{-1}\mathbf{r})^{\frac{1}{2}}}{(\det K^{-1})^{\frac{1}{4}}}. \tag{5.3}$$

This analytical solution is derived from (5.2) using the transformation of space variables (5.1). In this case the well model can be written as follows

$$p_w = p_0 + \frac{\mu}{(\det K)^{\frac{1}{2}}\rho}\frac{Q}{2\pi H}\ln\left(\frac{\tilde{r}_w}{\tilde{r}_0}\right) + \frac{\beta Q|Q|}{\rho(2\pi H)^2}\left(\frac{1}{\tilde{r}_0} - \frac{1}{\tilde{r}_w}\right),$$

where $\tilde{r}_w$ is the mean well radius computed according to [11].

$$\tilde{r}_w = \frac{1}{2}\left(\mathrm{cond}(K)^{\frac{1}{4}} + \mathrm{cond}(K)^{-\frac{1}{4}}\right) r_w = \frac{r_w}{2\pi}\int_0^{2\pi}\left(\frac{(\mathbf{z}^T K^{-1}\mathbf{z})}{(\det K^{-1})^{\frac{1}{2}}}\right)^{\frac{1}{2}} d\,\phi,$$

where $\mathbf{z}^T = (\cos(\phi), \sin(\phi))$. Now the calibration procedure is modified as follows: (a) fix constants R and p_R; (b) solve discretized equations in a "window" around the well with Dirichlet BC specified by (5.3); (c) find pressure p_0 in the well block and find $\tilde{r}_0$ as a solution to nonlinear system (5.3) using the equality $p(\tilde{r}_0) = p_0$. It is important that the physical properties for the calibration procedure should be the same as for the reservoir simulation, i.e., the Forchheimer number or its generalizations should be the same in both cases.

6 Numerical Experiments

Typical well model validation scenario requires the following stages: a) derivation of the well model; b) numerical experiments with flow around isolated well; c) numerical simulation of 5-spot flow on Cartesian/distorted grids using well models; d) validation using direct simulation of the 5-spot flow on extremely refined radial grids near wells. Table 2 shows the comparison of computed data on 201×201 grid with analytical solutions which clearly shows that the multiple-cell production terms result in more accurate solutions.

Scheme	$\frac{\|\|p_h - p\|\|_{L_1}}{\|\|p\|\|_{L_1}}, \%$	$\frac{\|\|p_h - p\|\|_{L_2}}{\|\|p\|\|_{L_2}}, \%$	$\frac{\|\|p_h - p\|\|_C}{\|\|p\|\|_C}, \%$
BFE	0.0049	0.039	0.41
BFE'	0.0074	0.164	2.31
FD	0.0060	0.079	0.93
CVFE'	0.0032	0.054	0.74
CVMFE	0.0026	0.018	0.23

Table 2. Discrete norms of errors for different schemes. (201×201 cells)

Injection rate	0.05 mmscf/day
Number of injection wells	4
Injection well coordinates (ft)	(0, 0) (200, 0) (0, 200) (200, 200)
Number of production wells	1
Production rate	4×0.05 mmscf
Production well coordinates (ft)	(100, 100)
Well radius	0.35ft
Reservoir dimensions	200 ft$\times$ 200 ft$\times$ 1 ft
Initial pressure, p_I	5000 psia
Fluid density	1.783926×10^{-1} g/cm^3
Fluid density	
at 1atm, 60^{o}F	$6.76361 \cdot 10^{-4}$ g/cm^3
Fluid viscosity	2.5574794×10^{-2} cp
$k_{11}, k_{22}(mD)$	10,10 or 10,100
$k_{12} = k_{21}$	0
Forchheimer coefficient β [ft^{-1}]	0, $1.71 \cdot 10^{10}$, $1.71 \cdot 10^{11}$
Boundary conditions	No-flow at all boundaries

Table 3. Simulation conditions.

Two different sample coarse grid configurations for the same 5-spot flow

are shown in Fig. 5

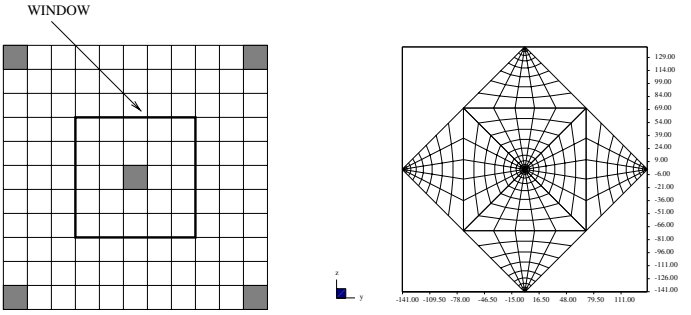

Figure 5: Different grids for 5-spot well configuration.

All data for this problem are presented in Table 3.

The well model validation results in the isotropic case for the CVMFE scheme are presented in Table 4. Production terms and well model are used on the 11×11 Cartesian grid while in direct simulation fluxes through well boundaries are specified. In this case the bottom-hole pressure p_w is the well model quality indicator. Very fine grids were used for direct simulation, typical cell size near well was about $r_w/50$.

β	$p_0 - p_I$	$r_0/\Delta x$	$p_w - p_I$	$p_w - p_I$, direct simulation	err %
0	-121.683	0.342926	-262.149	-262.602	0.17
$1.71 \cdot 10^{10}$	-132.067	0.35065	-490.176	-490.694	0.11
$1.71 \cdot 10^{11}$	-225.451	0.37137	-2542.4	-2543.5	0.04
$1.71 \cdot 10^{11}$			-2560 [6]		

Table 4. Comparison of simulation results.

b	β	$p_0 - p_I$	$r_0/\Delta x$	$p_w - p_I$	$p_w - p_I$, direct simulation	err %
0	$1.71 \cdot 10^{11}$	-387.46	0.376743	-2543.1	-2543.5	0.01
0.43	$1.71 \cdot 10^{11}$	-402.745	0.358036	-2543.1	-2543.5	0.01

Table 5. Results for the distorted grid simulations.

The numerical results illustrating the influence of the grid distortion on the accuracy of the calibration procedure in the isotropic case are presented in Table 5. Here $b\Delta x$ is the value of the quasi-random displacement for the

grid nodes. The initial 23×23 Cartesian grid and the resulting distorted grid are shown on Fig. 5.

Both grids along with discrete pressure and pressure errors are presented on Fig. 6. The pressure errors for the 5-spot flow are computed via comparison with very fine grid results.

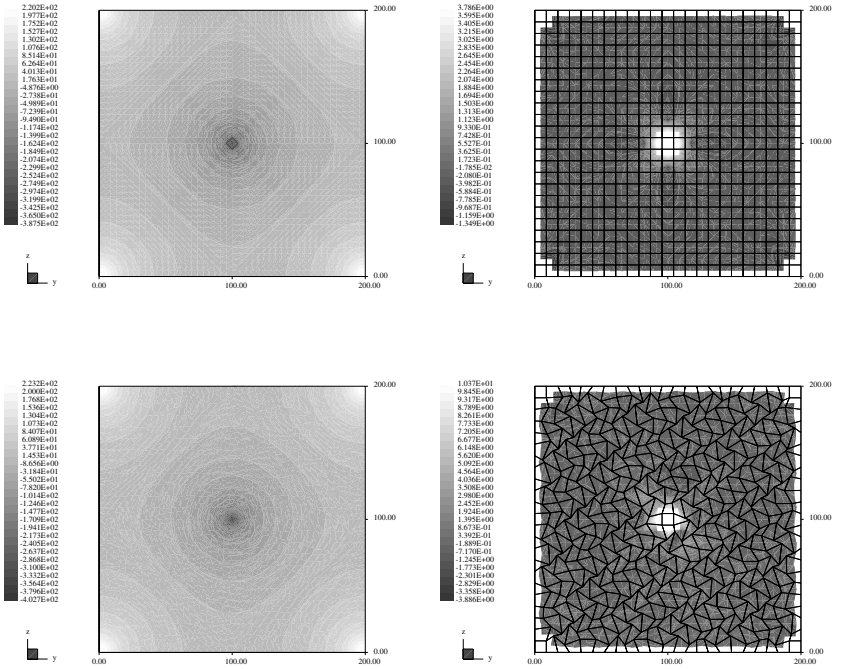

Figure 6: Pressure contour maps and error maps for regular and distorted grid simulations.

The pressure errors are only 3 times larger as compared to the results on square-cell grids. This is quite good, given that the distorted grid contains a lot of poorly shaped and non-convex cells.

The well model validation in the anisotropic case is more difficult since the normal flux distribution through the well boundary is not known. Hence in direct simulation p_w from the well model is specified while the predicted Q becomes the quality measure. Another observation is that as a rule of thumb the window around the well in the calibration procedure should be much larger as compared to the isotropic case for the same well model accuracy. The preliminary results of simulation on the 47×47 grid with square cells

are presented in Table 6.

β	$r_0/\Delta x$	$p_w - p_I$	exact Q	predicted Q	err %
$1.71 \cdot 10^{11}$	0.46	-2072	0.2	0.20015	0.076

Table 6. Validation results for $k_{11} = 10, k_{22} = 100$.

7 Conclusions

Asymptotic methods and the superposition principle allow the derivation of exact expressions for the equivalent radius r_0 for various approximation schemes on Cartesian grids.

An inexpensive black-box calibration procedure allows r_0 to be computed in general grid configurations for non-Darcy flows, including anisotropic cases.

The CVMFE approximation scheme provides optimal resolution for near-well flow, including the case of distorted grids. The derivation of CVMFE via low-order "cancellation" quadrature rules for MFE integrals can improve accuracy on highly distorted grids and can make the admissible set of grids in 2-D and 3-D much wider.

Direct simulation of Forchheimer flows is very expensive with high order approximation schemes being desirable.

Acknowledgments: This work was supported by Mobil Technology Company. We are grateful to I.E. Kaporin for providing the linear solver used in this work and for drawing our attention to the papers by V.B. Andreev. Partial support of research of the first author by NWO grant 047003017 is gratefully acknowledged.

References

[1] Andreev, V. B. and Kryakvina, S. A., The fundamental solution of a one-parameter family of difference approximations of the Laplace operator in the plane, *Zh. Vychisl. Mat. Mat. Fiz* **13** (1973), 343–355.

[2] Axelsson, O. and Gustaffson, I., An efficient finite element method for nonlinear diffusion problems, *Bull. Greek Math. Soc.* **32** (1991), 45–61.

[3] Basniev, K. S., Kochina, I. N., and Maksimov, V. M., *Underground hydromechanics*, Moscow, Nedra. 1993.

[4] Cai, Z., Jones, J. E., McCormick, S. F., and Russel, T. F., Control-Volume Mixed Finite Element Methods, *Computational Geosciences* **1** (1997), 289–315.

[5] Chavent, G. and Jaffre, J., *Mathematical models and finite elements for reservoir simulation*, North-Holland, 1986.

[6] Ewing, R. E., Lazarov, R., Lyons, S. L., Papavassiliou, D. V., Pasciak, J., and Qin, G., Numerical Well Model for Non-Darcy Flow through Isotropic Media, *ISC Research Report ISC-98-11-MATH* (1998).

[7] Forchheimer, P., Wasserbewegung durch Boden *Zeit. Ver. Deut. Ing.* **45** (1901), 1781–1788.

[8] Garanzha, V. A. and Konshin, V. N., *Approximation schemes and discrete well models for the numerical simulation of the 2-D non-Darcy fluid flows in porous media* Comm. in Appl. Math., Computing Center RAS, 1999.

[9] Knupp, P. and Lage, J., Generalization of Forchheimer-extended Darcy flow model to tensor permeability case via a variational principle, *J. Fluid Mech.* **299** (1995), 97–104.

[10] Peaceman, D. W., Interpretation of well-block pressure in numerical reservoir simulation, *SPE Paper 6893, SPE Journal, Trans. AIME* **253** (1978), 183–194.

[11] Peaceman, D. W., Interpretation of well-block pressures in numerical reservoir simulation with non-square grid blocks and anisotropic permeability, *SPE Journal* (1983), 531–543.

[12] Raviart, P. A. and Thomas, J. M., *A mixed finite element method for 2nd order elliptic problems. Mathematical aspects of the finite element method. Lecture notes in Mathematics*, **606**, Springer, 1977.

[13] Samarskii, A. A., Koldoba, V. A., Poveshchenko, Yu. A., Tishkin V. F., and Favorskiy, A. P., *Difference Schemes on Irregular Grids*, Minsk, 1996, (in Russian).

[14] Thauvin, F. and Mohanty, K. K,, *Modeling of non-Darcy flow through porous media*, SPE paper 38017, presented at 1997 SPE Res. Simulation Symp., Dallas, Texas, USA, 8-11 June, 1997.